Skeletal Muscle

METHODOLOGY

Open Access

Regenerative Index: a method to assess muscle regeneration in patients with Duchenne muscular dystrophy

Johnathan K. Smid[1,4], Charis A. McPherson[1], Jacob G. Monast[1], Shanti S. S. Rayagiri[1,4], Steven A. Moore[2] and Michael A. Rudnicki[1,3,4*]

Abstract

Background Duchenne muscular dystrophy (DMD) is a devastating disease manifested in skeletal muscle by repetitious myonecrosis and regeneration. Because the regenerative process is closely linked to the cumulative severity of muscle damage, which is variably distributed within and between muscle groups, accurately quantifying muscle regeneration has remained a significant challenge.

Methods Myofibers are delineated by immunostaining for laminin, and subsequent image analysis employed to generate a masked outline precisely within each myofiber boundary. Morphometric parameters including minimal Feret's diameter, cross-sectional area, and circularity were measured for each myofiber. In addition, the number of Pax7-expressing satellite cells were quantified. To evaluate regenerative activity, newly formed myofibers were identified by immunostaining for expression of embryonic myosin heavy chain (eMHC). Necrotic myofibers were enumerated by immunofluorescent detection of immunoglobulin G (IgG) infiltration. The Regenerative Index (RI) was calculated as the number of regenerating ($eMHC^+$) myofibers divided by the number of necrotic (IgG^+) myofibers. Determination of RI was performed on muscle biopsies obtained from 10 boys with DMD and 3 age-matched non-DMD controls.

Results A trend toward an increasing minimal Feret's diameter, cross-sectional area and circularity was observed with increasing age in DMD boys, with circularity showing the strongest trend. Furthermore, compared to DMD boys 7- to 8-years old, the boys 9- to 11-years old had increased myofiber circularity. Pax7-expressing cells per myofiber were elevated in DMD boys compared to control boys of similar ages, without any observation of age-related changes. The Regenerative Index in DMD boys exhibited a decline between 7 and 11 years of age, with an inverse correlation between RI and age.

Conclusions The use of eMHC and IgG immunostaining to calculate RI appears to provide a way to assess regeneration across biopsies that differ in histopathologic severity. Using this approach, RI showed a negative correlation with age in DMD boys aged 7 to 11 years which requires further investigation.

*Correspondence:
Michael A. Rudnicki
mrudnicki@ohri.ca

Full list of author information is available at the end of the article

Keywords Regenerative Index (RI), Muscle regeneration, Duchenne muscular dystrophy (DMD), Dystrophin, Embryonic myosin heavy chain (eMHC), Regenerating myofibers, Necrotic myofibers

Background

Duchenne muscular dystrophy (DMD) is a severe X-linked neuromuscular disorder caused by pathogenic variants in the *dystrophin* gene leading to an absence or non-functional dystrophin protein [1, 2]. Although still considered a rare disease, DMD is one of the most common forms of muscular dystrophy with a prevalence of 1:5,000 boys [3, 4]. Furthermore, it is one of the most severe forms of muscular dystrophy with a dramatic decline in abilities at a young age and a loss of independent walking in the pre-teen to early teenage years [5]. Although current standards of care and emerging gene-targeting therapies for DMD can prolong ambulation and improve survival into adulthood, the disease remains relentlessly progressive, and most continue to experience life-limiting respiratory and/or cardiac complications preventing a normal lifespan [6]. Taken together, there is an urgent need for more effective and widely accessible treatments for DMD.

Previous studies characterizing the trajectory of DMD myopathology have highlighted the lack of muscle regeneration [7, 8]. Moreover, intrinsic deficits from the lack of dystrophin in muscle stem cells has been shown to contribute to disease progression [9–13]. However, some studies report preserved regeneration capacity under specific conditions [14–16]. The importance of symmetric clonal expansion of satellite cells during the initial phase of regeneration has been demonstrated in zebrafish [17, 18]. Asymmetric divisions were also found to be a feature of muscle regeneration in zebrafish [19]. In *mdx* mice, the mouse model of DMD, the lack of dystrophin results in reduced polarity and the loss of asymmetric divisions [9], a key mechanism through which muscle stem cells maintain a pool of progenitor cells to facilitate regeneration [20]. This impairment results in reduced muscle regeneration, the senescence of muscle stem cells, and an accumulation of fibro-adipogenic progenitors [7, 21, 22]. A treatment to rescue this satellite cell defect and restore regeneration holds promise to be of therapeutic benefit [23].

A method to determine the efficacy of regeneration-enhancing therapeutics is currently lacking. To properly evaluate the effectiveness of such treatments, a biomarker specific to the quantification of muscle regeneration in response to degeneration would be critical. Biomarkers commonly employed in DMD trials, such as such as levels of muscle fiber dystrophin or reductions in markers of muscle fiber injury, are inadequate for evaluating interventions that enhance muscle regeneration, as these endpoints fail to capture improvements in regenerative capacity.

Evaluation of the general appearance of muscle using Haematoxylin and Eosin (H&E) staining has been the gold standard for muscle tissue assessment, as it can provide information on both degenerative and regenerative processes. Degeneration can be denoted by myonecrosis, the inflammatory response, and endomysial fibrosis, while manifestations of regeneration include basophilic sarcoplasm, increased variability in myofiber size, and internally-placed nuclei [24]. Nevertheless, H&E has several caveats when used alone for evaluating muscle degeneration and regeneration. Interpretation can be subjective and dependent on observer experience, which can introduce variability in scoring both myonecrosis and regeneration [24]. Furthermore, the multifocal nature of muscle damage, and variability within and between muscles compounds the challenge. Thus, a robust, objective method for quantifying both muscle regeneration and degeneration is essential to minimize subjectivity in scoring.

Embryonic myosin heavy chain (eMHC) has long been used to identify newly forming myofibers [25]. Moreover, quantification of the percentage of regenerating myofibers reveals a negative correlation with functional motor score in DMD and Becker muscular dystrophy (BMD) patients [26]. Evaluation of regeneration alone does not provide a complete representation as it comes in response to the myonecrosis occurring in these patients.

Myofiber necrosis can be quantified by the immunodetection of Immunoglobulin G (IgG) infiltration into myofibers due to loss of membrane integrity [27]. IgG and serum albumin are the two most abundant circulating proteins in the blood accounting for 80–90% of total plasma protein, binding together and persisting for about 3 weeks in humans [28]. Reliance on these markers are necessary as Evans blue dye (EBD) cannot be injected to determine necrotic fibers as done to identify myonecrosis in the mdx mouse. Alternative to IgG, the use of Albumin could be used to identify necrotic fibers as done in dystrophic mdx mice [29]. However, extensive variability in muscle fiber loss resulting from the variable myonecrosis and regeneration within and between muscles limits the utility of any determination of the rate of regeneration. To address this issue, we developed a quantitative measure of muscle regenerative activity, which we term the Regenerative Index (RI). Using this approach, regeneration is normalized to myonecrosis, which reduces variability arising from biopsy heterogeneity. The RI is defined as the ratio of newly formed ($eMHC^+$) myofibers

to necrotic (IgG^+) myofibers, thus normalizing the variation found between biopsies. Accordingly, the RI integrates both regenerative and degenerative states to assess the net regenerative potential of muscle. We propose that determination of RI may allow the monitoring of changes in the ability of DMD muscle to regenerate and thus could provide a useful tool to assess treatments enhancing muscle regeneration.

Methods

To develop a method to quantify a regenerative index in DMD and non-DMD, no histopathologic diagnostic abnormality controls (CTRL), muscle biopsy cryosections were stained and quantified using the methods outlined below. All muscle samples from biopsies performed at ages of 7 to 11 years old were obtained from the Repository at the University of Iowa Wellstone Muscular Dystrophy Specialized Research Center (IRB ID#200510769; original approval on 02/16/2006; most recent continuing review approval on 11/11/2025; see Table 1). Samples were received as frozen 10 µm sections on glass slides. All sections remained frozen until the time of immunostaining. Biopsies for the study were obtained from 2000 to 2024 and none of these individuals were participants in clinical trials. Specific information about corticosteroid treatment is not available, which is a limitation of the study. We cannot be certain but perhaps all these patients were receiving the standard of care therapy at the time of their muscle biopsy, which would have included corticosteroids.

Dystrophin Immunofluorescence

To determine the presence or absence of dystrophin, msIgG2b Dystrophin 4C7 (Santa Cruz, Cat#sc-33697) was prepared at a 1:100 dilution. This antibody binds to an epitope at the n-terminus of dystrophin that is coded by exon 1 of the *DMD* gene. Slides were incubated with primary antibodies for 1 h at room temperature (RT) followed by three washes with phosphate-buffered saline (PBS). The secondary antibody Goat Anti-mouse IgG2b Alexa Fluor 488 (Catalog# 21141) was prepared in PBS at a concentration of 1:1000. Secondary antibodies were incubated at RT for 30 min. After incubation slides were washed five times with PBS before adding 4′,6-diamidino-2-phenylindole (DAPI) for 5 min. After coverslipping slides with PermaFluor aqueous mounting medium (Fisher scientific, cat# TA030FM), each complete muscle biopsy section was scanned on a Zeiss Axio Observer Z1/7 microscope. In parallel, non-DMD sections were stained as a positive control (Supplemental Fig. 1).

Morphometric analysis of myofibers

Zen Image analysis software (Zeiss Zen version 3.7) was used to quantify myofiber dimensions. Briefly, the basal lamina border of each myofiber was delineated by fluorescent laminin immunostaining (Fig. 1a, b) and image analysis software provided a trace within the laminin staining (Fig. 1c). Zen image analysis software provided the cross-sectional area (CSA), minimal fiber ferret (MFF) and circularity measurements of each myofiber. The quantification is semi-automated, with the software automatically performing all traces according to operator specifications, followed by minor manual edits to split myofibers that the software has merged or add in parts of the myofiber which were mis-selected. Further analysis of data exported from the Zeiss image analysis software was carried out with Graphpad Prism (version 10.4.1) and Microsoft Excel (version 16.89).

Pax7 immunofluorescence and quantification

To identify PAX7-expressing satellite cells mouse IgG1 anti-Pax7 hybridroma (DSHB) was thawed at 37 ºC and

Table 1 List of muscle samples with age, muscle type and *DMD* variant, if known

Sample ID	Age	Muscle	DMD variant
DMD18	7	Quadriceps	not known
DMD29a	7	Quadriceps	c.4237delA, p.Ile1413Serfs*5
DMD33a	8	Quadriceps	29 kb deletion of intron 44 and all of exon 45
DMD58a	8	Quadriceps	exon 19 out of frame deletion that causes frameshft p.Ala765Argfs*15
DMD5a	8	Quadriceps	c.6537dupT, p.Ile2180Tyrfs*43
DMD36	9	Quadriceps	not known
DMD9	9	Anterior tibialis	c.457 C > T, p.Gln153*
DMD28	10	Unknown	not known
DMD44b	10	Quadriceps	ex 38–43 out of frame deletion that causes a frameshift p.Ser1777Ilefs*2
DMD32	11	Anterior tibialis	c.457 C > T, p.Gln153*
CTRL12	8	Quadriceps	none
CTRL77a	10	Quadriceps	none
CTRL76	11	Unknown	none

DMD Duchenne muscular dystrophy, *CTRL* Control (non-DMD)

The* identifies a stop codon

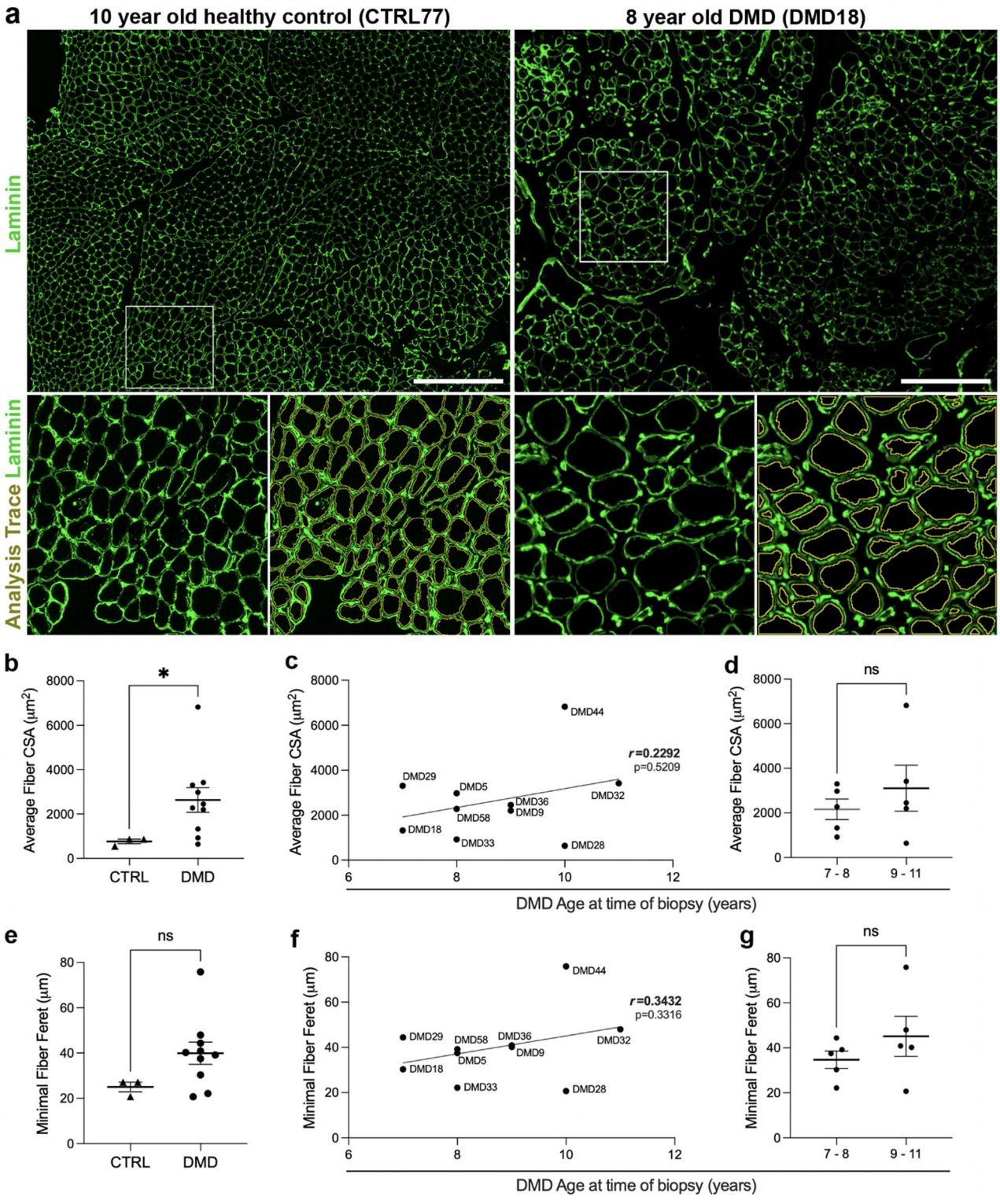

Fig. 1 (See legend on next page.)

(See figure on previous page.)

Fig. 1 Fiber size in DMD muscle samples relative to non-DMD controls. **a** Representative laminin 111 fluorescent immunostaining (green) of a 10-year-old healthy control (CTRL77) and an aged-matched DMD patient (DMD44), with 500 µm insets showing the corresponding analysis traces to illustrate automated segmentation of individual fibers. Scale bar = 500 µm (**b**) Quantification of average fiber cross-sectional area (CSA) shows significantly larger fibers in DMD compared with non-DMD controls (unpaired nonparametric Mann-Whitney test). **c** Average fiber CSA plotted against age at biopsy in DMD patients reveals a weak, non-significant positive correlation ($r = 0.2292$, $p = 0.5209$; Spearman correlation analysis). **d** Similarly, comparison of younger (7–8 years) and older (9–11 years) DMD patients shows no significant difference in average fiber CSA (ns, unpaired t test). **e** DMD muscle samples exhibit a significant increase in minimal fiber Feret diameter (MFF) compared to non-DMD controls (*$p < 0.05$, unpaired nonparametric Mann-Whitney test). **f** Correlation between MFF and age remains weak ($r = 0.3432$) and has a non-significant correlation ($p = 0.3316$; Spearman correlation analysis). **g** Likewise, there is no significant difference in MFF observed when comparing younger (7–8 years) and older (9–11 years) DMD patients (ns, unpaired t test)

vortexed for 20 s. Rabbit anti-Laminin (Sigma, cat#L9393) was added to the Pax7 hybridoma for a final concentration of 1:1,000. Slides were incubated with primary antibodies for 1 h at RT followed by three washes with PBS. The secondary antibodies anti-rabbit A488 (Invitrogen, cat# A11008) and anti-mouse IgG1 A546 (Invitrogen, cat# A21123) were prepared in PBS at a concentration of 1:1000. Secondary antibodies were incubated at RT for 30 min. After incubation slides were washed five times with PBS, stained for DAPI, and mounted with coverslips as described above. The complete muscle biopsy section was scanned on a Zeiss Axio Observer Z1/7 microscope. Quantification was performed with Zeiss image analysis software by first identifying the nucleus with DAPI and then setting a threshold to determine if the nuclei is $Pax7^{+ve}$. Quantification was performed in a semi-automated manner, with each section visually inspected to identify false positives in regions of high background. The total number of $Pax7^{+ve}$ cells in the quantified area of the biopsy was divided by the total number of fibers in that area of biopsy to determine $Pax7^{+ve}$ cells per myofiber.

Pipeline for Regenerative Index (RI) measurement

Immunofluorescent staining was performed to identify IgG + and eMHC+ myofibers with Mouse IgG2a anti-human IgG mAb (Abcam, Cat# ab200699) and Mouse IgG1 anti-eMHC mAb (Santa Cruz, Cat# sc-53091) were prepared in PBS at a dilution of 1:200. In addition, to identify myofiber membranes Rabbit Anti-Laminin (Sigma, Cat# L9393; binds to laminin 111) was also added at a dilution of 1:1,000. Slides were incubated with primary antibodies for 1 h at RT followed by three washes with PBS. The secondary antibodies Goat Anti-Mouse IgG2a Alexa Fluor 488 (Invitrogen, Cat# A21131), Goat Anti-Mouse IgG1 Alexa Fluor 546 (Invitrogen, Cat# A21123) and Goat Anti-Rabbit Alexa Fluor 647 (Invitrogen, Cat# A21244) were prepared in PBS at a concentration of 1:2000. Secondary antibodies were incubated at RT for 30 min. After incubation slides are washed five times with PBS before adding DAPI for 5 min before adding mounting media and a coverslip.

Whole-biopsy imaging was performed by scanning the complete muscle biopsy on a Zeiss Axio Observer Z1/7 microscope. In parallel, sections stained with secondary antibodies only were also imaged to validate the specificity of staining (Supplemental Fig. 2). Importantly, throughout all steps of the analysis pipeline the quantification was done blinded to the age of the muscle biopsy.

Selection of quantification area was performed in Zen Image Analysis Software on whole-biopsy images taken with the Zeiss microscope. This is done by selecting frames around the areas to be quantified, leaving out any area that is unquantifiable due to tissue folds or areas with high in autofluorescence. This is an important step in the interactive analysis to remove any areas that would give high numbers of autofluorescence.

Laminin mask generation is then performed by creating a segmentation mask based on laminin staining to define fiber boundaries. This automatic segmentation allows the user to set optimal initial parameters for size and shape of fibers. The parameters of size, smoothing, fill holes, dilate, erode and morphology are adjusted in each image analysis to achieve optimal object selection. When necessary, this is followed by an interactive segmentation where fiber boundaries can be drawn, erased, cut or connected.

Signal quantification is performed by measuring IgG and eMHC fluorescence intensities within the laminin-defined mask. The fluorescent intensity within the myofiber boundary was measured with the same software to aid in the identification of either IgG + or eMHC+ myofibers. A representative image of a quadricep muscle is shown stained with IgG and eMHC (Fig. 4a).

Fiber classification guided by the calculated intensities are then performed to determine the total number of myofibers, as well as the number expressing eMHC and IgG. This allows for the calculation of the individual percentage of both the eMHC + and IgG+ over total number of myofibers. Moreover, this allows for the Regenerative Index (RI) to be calculated as the total number of eMHC immunostained myofibers divided by the total number of IgG immunostained myofibers.

Statistical analysis

Statistical comparisons between two groups were performed using an unpaired nonparametric Mann–Whitney test, as normality of distribution cannot be assumed. Similarly, correlation analyses were conducted using Spearman correlation to assess the strength of association between variables and determine significance

without assuming a Gaussian distribution. All statistical analysis was carried out with GraphPad Prism (version 10.4.1).

Results

Histological analysis of disease progression in DMD

We conducted our analysis on DMD patients from 7- to 11-years of age because these patients are the focus of many clinical trials [30] as they typically are initially ambulatory and lose ambulation within four years [5, 31]. Representative H&E photomicrographs from each DMD biopsy and from one non-DMD control are shown in Supplemental Fig. 3. We examined the standard markers for disease progression including cross-sectional area (CSA), mean fiber Feret (MFF), and circularity of myofibers [24, 32–34]. Moreover, we examined the abundance of satellite cells by immunofluorescent detection of Pax7 to gain insight into the regenerative process.

DMD muscle samples displayed a significantly elevated average myofiber cross-sectional area (CSA) compared to age-matched healthy muscle biopsies (Fig. 1a, b). Although myofiber CSA demonstrated a trend toward increased values with age, variability across DMD samples yielded a weak correlation (low ***r*** value) with age which was not significant (Fig. 1c). The mean coefficient of variation increased from 23.4% in the Control to 66.5% in DMD. In addition, comparing the average of all five 7–8-year-old DMD samples to the average of five samples from 9-11-year old patients did not show a statistically significant difference (Fig. 1d).

The minimal fiber Feret (MFF) or the minimal Feret's diameter is the smallest distance between two parallel tangents to the myofiber cross-section and can be a robust measure of myofiber size as the error from non-perpendicular sectioning is reduced [35]. However, the MFF of DMD samples did not show a significant increase when compared to healthy controls (Fig. 1e) and substantial variability resulted in a weak (low *r*), non-significant age-MFF correlation (Fig. 1f). No statistically significant difference in MFF was observed between DMD samples from 7–8-year-old versus 9-11-year-old patients (Fig. 1g).

Examination of circularity revealed that there was a statistically significant shift in distribution of circularity in older versus younger boys with a stronger correlation than MFF or CSA (Fig. 2). Notably, the mean circularity was higher in muscle biopsies from 9–11-year-olds compared with 7–8-year-old DMD boys (Fig. 2b, c). Moreover, increased circularity was observed in areas with increased endomysial space (Fig. 2a, bottom insets) when compared to more tightly packed myofibers (Fig. 2a, top insets). In non-DMD muscle, where endomysial space is greatly reduced, there was decreased circularity (Supplemental Fig. 4). However, the high variability observed in younger boys resulted in a weak non-significant correlation with age (Fig. 2d).

PAX7 staining was combined with laminin to enumerate satellite cells in both DMD and non-DMD control (CTRL) muscle samples from patients 7–11 years of age (Fig. 3a). Quantifying the number of PAX7-expressing cells and the number of myofibers revealed a significant increase in the number of PAX7-expressing satellite cells in DMD samples relative non-DMD controls (Fig. 3b). There was no decrease in satellite cell number as the boys aged and in fact there was a trend of an increase (Fig. 3c), without any significant difference when comparing 7–8 years with 9–11 years (Fig. 3d). Additional representative images with Pax7 staining are shown in Supplemental Fig. 5.

Taken together, using several standard approaches to quantify DMD disease progression, we observed little or no correlation with age likely due to the high variability between samples and patients.

Determination of Regeneration Index

To normalize the variable degrees of myonecrosis and regeneration that occur within and between muscles in DMD patients, we developed a measure of muscle regenerative capacity, which we term the Regenerative Index (RI). The RI is the ratio of newly formed ($eMHC^+$) myofibers over necrotic (IgG^+) myofibers.

To accurately quantify the dynamic balance between myonecrosis and regeneration we combined laminin immunostaining with staining for IgG or eMHC (Fig. 4a). Following the same laminin trace analysis performed to calculate CSA and MFF, regenerating myofibers were identified and enumerated based on eMHC expression and necrotic myofibers were identified and enumerated based on IgG staining. The complete list of quantified values and calculated RI are listed in Table 2. Notably, non-DMD control samples exhibited minimal to no detectable eMHC or IgG staining (Supplemental Fig. 6).

Enumeration of regenerating ($eMHC^+$) or necrotic (IgG^+) revealed age-related trends in muscle regeneration and degeneration. The percentage of $eMHC^+$ myofibers showed a weak negative correlation with age at biopsy (r = -0.4459, $p = 0.1975$), indicating trend between increasing age and a reduced proportion of regenerating myofibers (Fig. 4b). In contrast, the percentage of IgG^+ myofibers showed a trend for a positive correlation with age ($r = 0.4707$, $p = 0.1714$) but did not reach statistical significance (Fig. 4c). Comparisons between younger (7–8 years) and older (9–11 years) groups showed no statistically significant differences in either $eMHC^+$ or IgG^+ myofiber percentages (Fig. 4d, e).

In striking comparison, determination of Regenerative Index (RI), defined as the ratio of newly forming $eMHC^+$ myofibers to necrotic IgG^+ myofibers (Fig. 5a), revealed

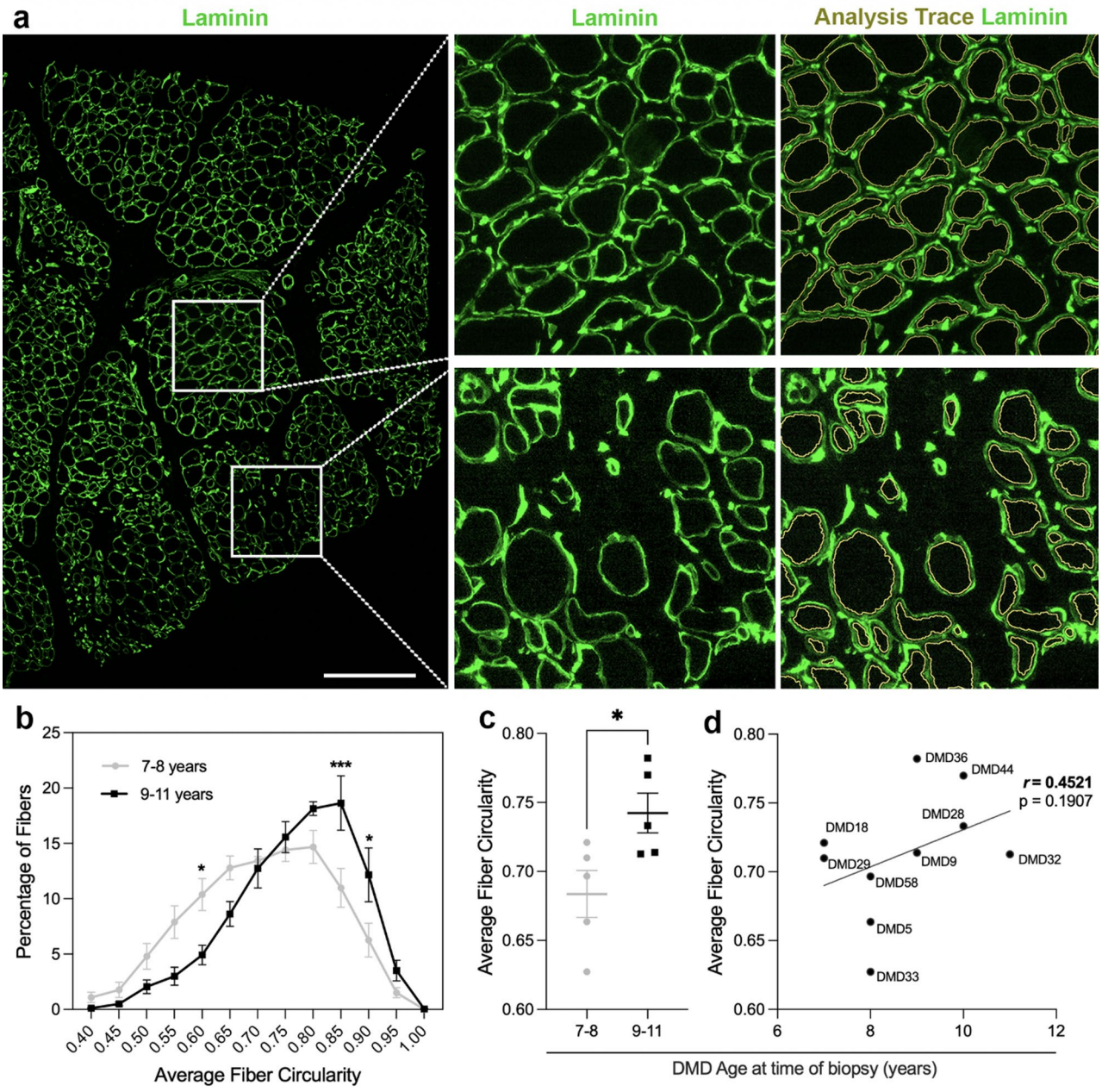

Fig. 2 Myofiber circularity is significantly increased in DMD muscle. **a** Representative laminin-immunostained DMD muscle section showing heterogeneous fiber shape with 500 µm insets including the image analysis trace in yellow. Scale bar = 500 µm. **b** Distribution of average fiber circularity in younger (7–8 years, grey) and older (9–11 years, black) DMD patients, showing a rightward shift toward more circular fibers in the older group. **c** Mean fiber circularity is significantly increased in older compared with younger DMD patients (unpaired nonparametric Mann-Whitney test, $*p < 0.05$). **d** Average fiber circularity shows a weak, non-significant positive correlation with age at biopsy in DMD patients (Spearman, $r = 0.4521$, $p = 0.1907$)

a strong inverse relationship with age at biopsy in boys with DMD (Fig. 5b). The RI decreased significantly with age (r = -0.9042, $p = 0.0006$), indicating a highly significant loss of regenerative capacity as boys grew older (Fig. 5b). Furthermore, comparison between age groups revealed that 7–8-year-old boys had a markedly higher RI than 9–11-year-olds, with the difference reaching high statistical significance (Fig. 5c).

This finding demonstrates that the regenerative potential in DMD muscle declines sharply with age, as measured by the Regenerative Index. The RI being a ratio, is effective at normalizing the variation found between biopsies and thus provides a useful approach to evaluate the efficiency of regeneration which occurs in response to myofiber damage that is focal and distributed in nature. Therefore, we propose that determination of RI could

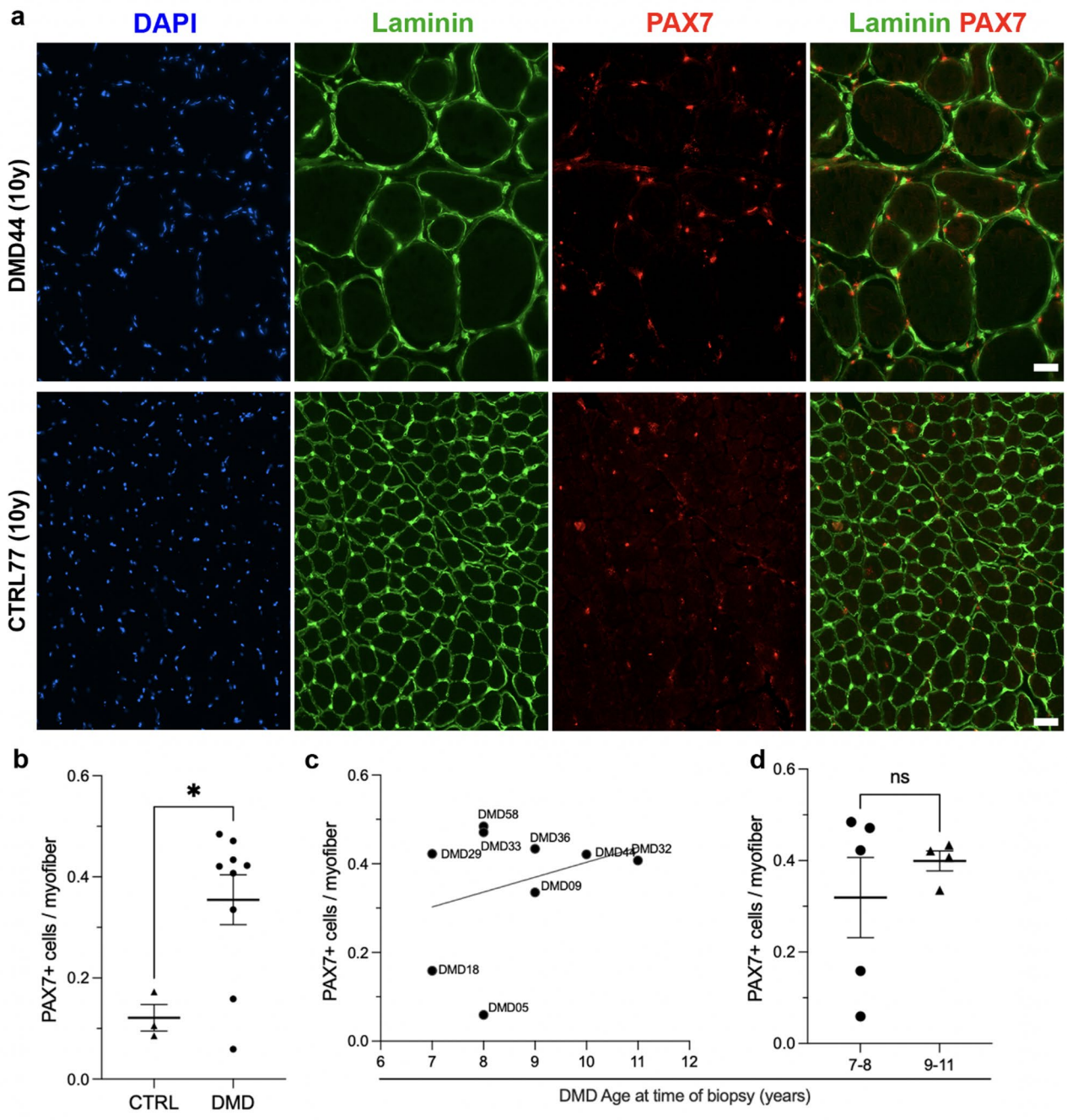

Fig. 3 PAX7⁺ satellite cells are increased in DMD muscle. **a** Representative sections of DMD (DMD44, 10 years) and age-matched control (CTRL77, 10 years) muscle stained for DAPI (blue), laminin (green), PAX7 (red), and laminin/PAX7 overlay. Scale bar = 50 µm. **b** Quantification shows a significant increase in PAX7⁺ cells per myofiber in DMD compared with non-DMD controls (CTRL) (unpaired nonparametric Mann-Whitney test). **c** In DMD biopsies, the number of PAX7⁺ cells per myofiber did not show any correlation when analyzed by Spearman correlation. **d** No significant difference in PAX7⁺ cells per myofiber is observed between younger (7–8 years) and older (9–11 years) DMD patients (ns, unpaired nonparametric Mann-Whitney test)

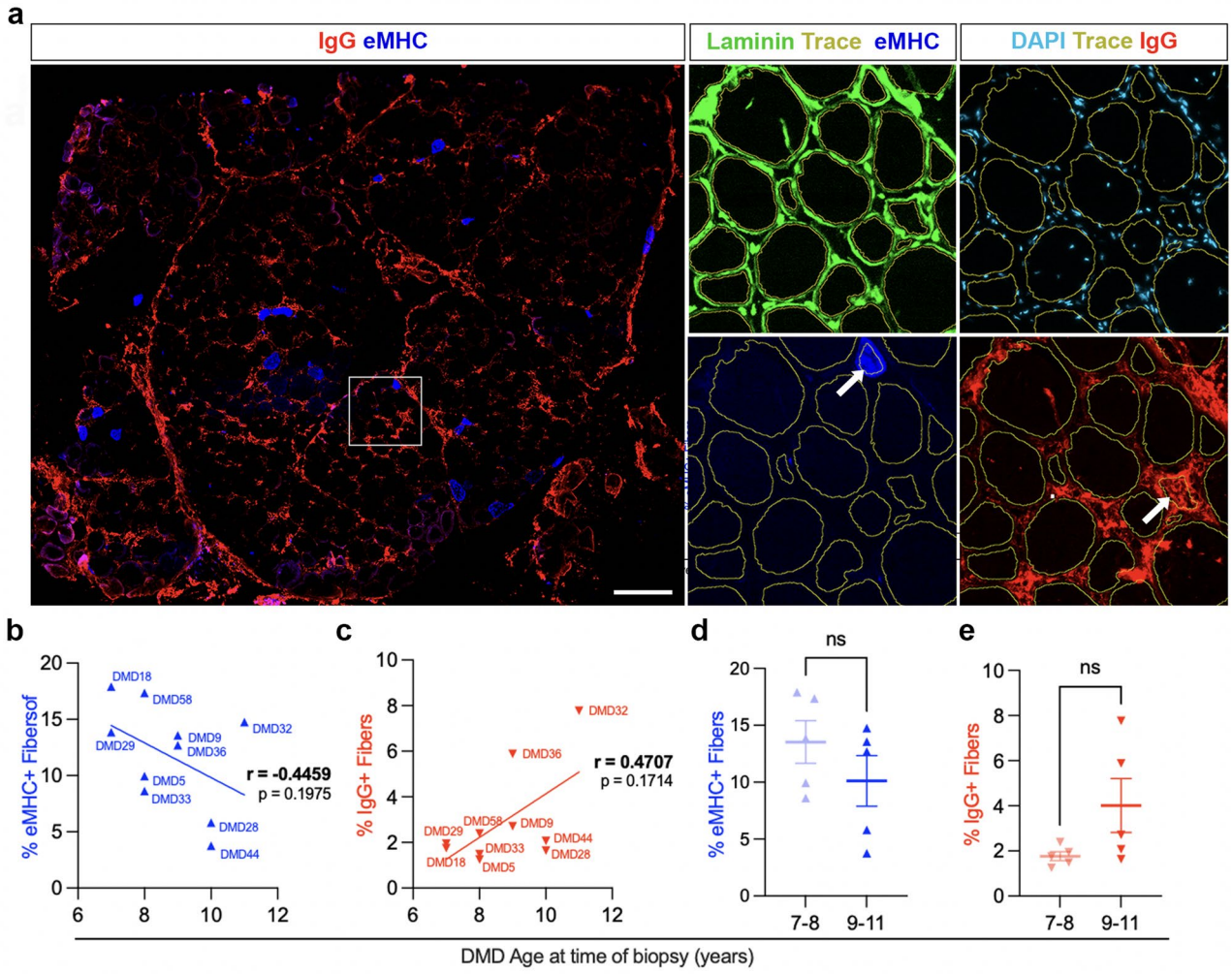

Fig. 4 Decreased regeneration and increased degeneration in DMD muscle. **a** Representative immunofluorescence image of a DMD muscle biopsy stained for IgG (red) and embryonic myosin heavy chain (eMHC, blue), with 500 µm insets showing laminin (green) and automated tracing traces outlining individual fibers (yellow) to determine presence or absence of either eMHC or IgG (see thick white arrows). **b** Percentage of eMHC⁺ fibers in individual DMD patients plotted against age at biopsy, showing a weak negative and not significant Spearman correlation (r = -0.4459, p = 0.1975). **c** Percentage of IgG⁺ fibers in DMD patients plotted against age at biopsy, indicating a trend toward increased IgG⁺ fibers with age that does not reach statistical significance with a Spearman correlation analysis (r = 0.4707, p = 0.1714). **d**, **e** Comparison of younger (7–8 years) and older (9–11 years) DMD patients shows no significant differences in the proportion of eMHC⁺ fibers (**d**) or IgG⁺ fibers (**e**) (ns, unpaired nonparametric Mann-Whitney test)

allow the monitoring of changes in the ability of DMD muscle to regenerate, providing a tool to assess treatments designed to enhance muscle regeneration.

Discussion

This study was designed to develop and test a quantitative method rather than to definitively establish clinical correlations. Notably, we observed a significant decline in the Regenerative Index (RI) between 7 and 11 years of age, despite relatively stable myofiber morphology and satellite cell numbers. Our findings thus suggest that RI may capture aspects of muscle regenerative activity that warrant further investigation. An inverse correlation between RI and patient age suggests that the muscle's ability to regenerate myofibers relative to ongoing myonecrosis deteriorates rapidly early in DMD. This early impairment in the efficiency of regenerative ability may correlate with the previously observed loss of satellite cell polarity in the absence of dystrophin [9, 23, 36]. These findings support the feasibility of quantifying concurrent degeneration and regeneration within DMD muscle biopsies. While preliminary trends suggest age-associated differences, larger studies with increased numbers and detailed clinical annotation will be required to determine whether this metric reflects disease progression of regenerative capacity.

In our studies, DMD satellite cell numbers per muscle fiber were increased relative to non-DMD controls without a significant reduction in abundance with increasing age. This aligns with earlier evidence suggesting that

Table 2 Regenerative Index quantification for 7–11 year DMD samples

Sample	Age	IgG$^+$ fibers	eMHC$^+$ fibers	RI	Total fibers	Percent IgG$^+$ fibers	Percent eMHC$^+$ fibers
DMD 18	7	48	492	10.3	2747	1.75	17.91
DMD 29	7	29	205.5	7.1	1484	1.95	13.85
DMD 33a	8	19	131	6.9	1520	1.25	8.62
DMD 58a	8	26	189	7.3	1089	2.39	17.36
DMD 05b	8	13	87	6.7	874	1.49	9.95
DMD 09	9	21	105	5.0	774	2.71	13.57
DMD 36	9	40.5	87.5	2.2	689	5.88	12.70
DMD 28	10	38	135	3.6	2324	1.64	5.81
DMD 44	10	17	31	1.8	822.5	2.07	3.77
DMD 32	11	156	324	2.1	2195	7.11	14.76
CTRL 12	8	0	0	undefined	6771	0.00	0.00
CTRL 77a	10	10	3	0.3	5721	0.17	0.05
CTRL 76	11	5	0	0.0	4737	0.11	0.00

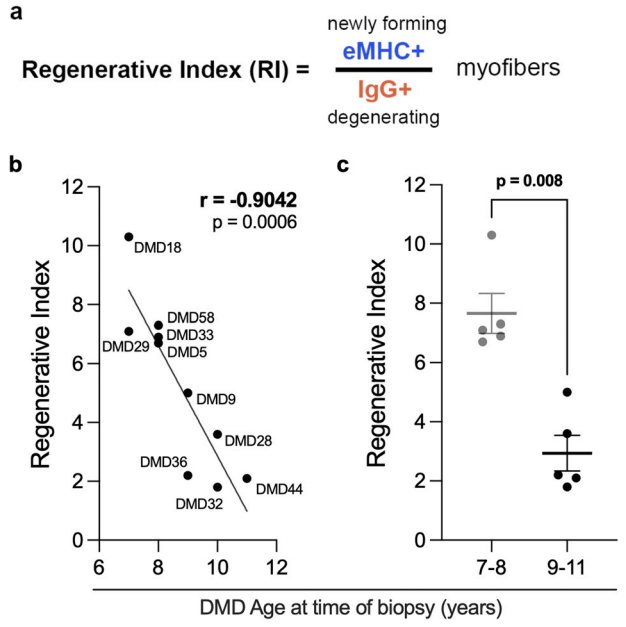

Fig. 5 Regenerative Index is significantly decreased in DMD boys between 7 to 11 years of age. **a** Schematic representation of the Regenerative Index (RI), defined as the ratio of newly forming eMHC-positive myofibers to necrotic IgG-positive myofibers. **b** Plot of RI versus age at biopsy in DMD patients, showing a strong negative correlation between regenerative index and age (r = -0.9042, p = 0.0006; Spearman correlation analysis). **c** Comparison of RI between younger (7–8 years) and older (9–11 years) DMD patients demonstrates a significantly higher regenerative index in the younger group (**$p < 0.002$, unpaired nonparametric Mann-Whitney test)

numbers of satellite cells remain elevated until much later in DMD [7]. However, the lack of dystrophin impairs satellite cell polarity resulting in their reduced ability to generate progenitors through asymmetric divisions [9]. A dysfunction in asymmetric satellite cell division may increase symmetric divisions, temporarily elevating total satellite cell numbers. However, if myogenic progenitors are reduced in parallel, the expected long-term result is impaired muscle regeneration. Both aging and repeated degeneration-regeneration cycles promote myofiber branching resulting in the increased numbers of small fibers [37, 38]. The abundance of small, branched myofibers derived from a parent fiber both complicates histological assessment of myofiber size and leads to overestimation of fiber number. However, despite this potential overestimation, the number of PAX7$^+$ satellite cells per fiber remains significantly increased.

A second negative effect of impaired satellite cell polarity may be increased chromosomal misalignment and mitotic catastrophe leading to satellite cells entering programmed cellular senescence [7, 9], and amplification of an inflammatory response [39, 40]. Correcting this polarity defect would maintain the number of progenitors associated muscle fiber regeneration. The RI measurement described here is a means by which therapeutics targeting DMD satellite cells may be evaluated.

One limitation of the Regenerative Index is the inability to compare DMD muscle samples directly to non-DMD controls. As these controls typically display no eMHC$^+$ or IgG$^+$ myofibers, the RI could be undefined, zero, or based on a very small number of myofibers. Conversely, therapies targeting dystrophin expression can be directly evaluated against placebo controls. Restoration of dystrophin to levels observed in healthy muscle represents the ultimate therapeutic goal. Dystrophin can be measured in both by either Western blot or quantitative immunofluorescence to determine therapeutic success. However, unlike the dystrophin measurement, muscle regeneration markers cannot be compared between DMD and healthy individuals, due to the inherent differences in regeneration activity and pathology between diseased and normal muscle. Regenerative marker expression reflects ongoing disease processes rather than basal healthy muscle status. This distinction underscores the complexity of using RI

as treatment benchmarks and shows the importance of longitudinal evaluation over time within DMD patients.

Although eMHC is downregulated as muscle fibers mature and become innervated, it has also been shown that it can be re-expressed in denervated muscle [25]. Moreover, denervation occurs in DMD [41] and in mdx mice [42]. Since denervated fibers may also express eMHC, additional criteria may help distinguish denervated from regenerating fibers. Interestingly, denervation was found to occur only in type 2A fibers [43] suggesting that fiber-type context may help refine interpretation. Muscle fiber size may also be informative, since smaller fibers are more consistent with regeneration, whereas larger eMHC-positive fibers may reflect denervation. Finally, diffuse acetylcholine receptors present in denervated skeletal muscle could be visualized by light and electron microscopy in muscle biopsy specimens [44]. Further quantification and exclusion of denervated eMHC-positive myofibers in DMD could therefore refine the Regenerative Index.

Changes in the extracellular matrix (ECM) influences satellite cell activation, attachment, differentiation and maturation to myotubes playing a major role in DMD [45–47] and aging [48, 49]. While regeneration is impaired by intrinsic satellite cell polarity defects [9], changes in the ECM may work synergistically to impair regeneration. Future integration of RI with ECM profiling could elucidate these interactions. Immunostaining for structural ECM proteins like collagen I/IV would allow for quantification of fibrosis in parallel to RI. This would allow the quantification of collagen density per field or % fibrotic area. Integrating this with RI could provide a RI-adjusted-for-fibrosis measure by simply multiplying the RI by the % of area that is not fibrotic. The ECM is not the only external modulator of regeneration. Inflammation-driven asynchronous remodeling [50] and pro-fibrotic macrophages in DMD and aging [51] have adverse effects on regeneration, potentially compounding a decline in RI. Future studies integrating immune profiling with RI will clarify these interactions. Moreover, inflammation-driven asynchronous remodeling [50] and pro-fibrotic macrophages in DMD and aging [51] have adverse effects on regeneration, potentially compounding a decline in RI. Future studies integrating immune profiling with RI will clarify these interactions. Dependent on sample availability, combining RI profiling with bulk or single-cell RNA sequencing on the same biopsy material would provide valuable context to the environment surrounding muscle fibers withing that sample including the quantification of immune cell infiltration. This would allow the addition of an immune modifier component to provide a context-adjusted regenerative capacity as well as linking changes in RI values to specific molecular pathways. Integrating both immune and ECM into the RI provides a context-adjusted measure of regenerative capacity that accounts for inflammatory and fibrotic barriers, improving biomarker accuracy and mechanistic interpretability for DMD assessment.

Therapies targeting satellite cell biology are emerging that may have potential in combination to therapies reintroducing dystrophin [52–54]. Evaluating such therapies will benefit from a method to more directly measure efficacy of increasing regenerative activity. While novel biomarkers of muscle regeneration would be highly valuable, and histological approaches offer precise insights, their acceptance, particularly within the pediatric population, may be tempered by practical considerations surrounding muscle tissue collection. Therefore, the efficacy of such biomarkers must substantially outweigh the burdens of muscle biopsy sampling to justify their clinical implementation. Previously it was shown that increased myofiber size was observed comparing pre- and post-treatment muscle biopsies [34]. However, knowing myofiber size also increases over time without therapeutic intervention makes this difficult to interpret. Thus, morphometric analysis falls short of proving the increase is from drug treatment alone. As demonstrated, RI declines from age 7 to 11, therefore an increase after treatment or even a maintenance of RI would be a convincing measure of efficacy.

Future longitudinal studies correlating RI with functional outcomes as well as examining RI across other muscle diseases and age groups will be important to validate and refine its use in clinical settings. Moreover, integrating transcriptomic and metabolic profiling with morphological indices like the Regenerative Index could refine our understanding of the mechanistic transitions underlying early regeneration failure in dystrophic muscle.

Conclusions

The Regenerative Index (RI) integrates both regenerative and degenerative states to assess the net regenerative potential of muscle. Compared to methods currently in use, RI may provide a quantitative measure of muscle regeneration that reflects ongoing regenerative activity in DMD. The age associated RI difference observed in our study suggests potential utility of the Index while also implying an early decline in regenerative potential despite the sustained satellite cell pool. Therapeutics to improve this regenerative capacity in DMD are a much-needed addition to future treatments. Future studies will investigate the utility of the Regenerative Index to provide a quantitative approach for evaluating the effectiveness of therapies aimed at improving muscle regeneration in conditions such as DMD.

Abbreviations

BMD	Becker Muscular Dystrophy
CTRL	Control (non-DMD)
CSA	Cross-sectional area
DAPI	4′,6-diamidino-2-phenylindole
DMD	Duchenne Muscular Dystrophy
DSHB	Developmental Studies Hybridoma Bank
ECM	Extracellular Matrix
eMHC	Embryonic Myosin Heavy Chain
H&E	Haematoxylin and Eosin
IgG	Immunoglobulin G
MFF	Minimal fiber Feret (minimal Feret's diameter)
Pax7/PAX7	Paired box protein 7 (satellite cell marker)
PBS	Phosphate-buffered saline
RI	Regenerative Index
RT	Room temperature

Supplementary Information

The online version contains supplementary material available at https://doi.org/10.1186/s13395-026-00436-3.

Supplementary Material 1.

Acknowledgements
The authors thank the University of Ottawa Imaging Core for use of microscopes and training required for scanning in entire muscle biopsy sections.

Authors' contributions
JKS and MAR designed research, analyzed data, and wrote the paper. CAM performed the RI and JGM the Pax7 staining and quantification. SSSR made contributions to the conception, data analysis and manuscript review. SAM provided all muscle biopsy cryosections, images of the histopathology, assisted with interpretation of the data, and edited the manuscript.

Funding
This study was supported by a research contract from Satellos Bioscience to MAR. SAM and the Iowa Wellstone Muscular Dystrophy Specialized Research Center muscle biopsy Repository are supported by grant P50NS053672 from the National Institute of Neurological Disorders and Stroke (NINDS).

Data availability
All data needed to evaluate the conclusions in the paper are present in the paper. Any additional information required to reanalyze the data reported in this work paper is available from the lead contact (mrudnicki@ohri.ca).

Declarations

Ethics approval and consent to participate
All muscle samples used in the study are biopsies from the Repository in the University of Iowa Wellstone Muscular Dystrophy Specialized Research Center. Approval to use them for research is covered in the IRB protocol ID#200510769 (original protocol approval on 02/16/2006; most recent continuing review approval on 11/11/2025).

Competing interests
MAR is the Founding Scientist and Chief Discovery Officer of Satellos Bioscience and receives consulting remuneration and holds stocks and options. SSSR is a Scientist and JKS is Director of Biology for Satellos Bioscience and both hold stock options. The remaining authors declare no conflict of interest.

Author details
[1]Sprott Centre for Stem Cell Research, Regenerative Medicine Program, Ottawa Hospital Research Institute, Ottawa, Canada
[2]Department of Pathology, Carver College of Medicine, University of Iowa, Iowa City, USA
[3]Department of Cellular and Molecular Medicine, Faculty of Medicine, University of Ottawa, Ottawa, Canada
[4]Satellos Bioscience, Toronto, Canada

Received: 23 December 2025 / Accepted: 26 June 2026
Published online: 01 July 2026

References

1. Hoffman EP, Brown RH Jr., Kunkel LM. Dystrophin: the protein product of the Duchenne muscular dystrophy locus. Cell. 1987;51(6):919–28.
2. Hoffman EP. The discovery of dystrophin, the protein product of the Duchenne muscular dystrophy gene. FEBS J. 2020;287(18):3879–87.
3. Kariyawasam D, D'Silva A, Mowat D, Russell J, Sampaio H, Jones K, Taylor P, Farrar M. Incidence of Duchenne muscular dystrophy in the modern era; an Australian study. Eur J Hum Genet. 2022;30(12):1398–404.
4. Guiraud S, Aartsma-Rus A, Vieira NM, Davies KE, van Ommen GJ, Kunkel LM. The Pathogenesis and Therapy of Muscular Dystrophies. Annu Rev Genomics Hum Genet. 2015;16:281–308.
5. Zambon AA, Ayyar Gupta V, Ridout D, Manzur AY, Baranello G, Trucco F, Muntoni F, Network UKNC. Peak functional ability and age at loss of ambulation in Duchenne muscular dystrophy. Dev Med Child Neurol. 2022;64(8):979–88.
6. Mah JK. Therapeutic options for Duchenne muscular dystrophy: hope or hype? Ther Adv Neurol Disord. 2025;18:17562864251346326.
7. Cardone N, Taglietti V, Baratto S, Kefi K, Periou B, Gitiaux C, Barnerias C, Lafuste P, Pharm FL, Pharm JN, et al. Myopathologic trajectory in Duchenne muscular dystrophy (DMD) reveals lack of regeneration due to senescence in satellite cells. Acta Neuropathol Commun. 2023;11(1):167.
8. Abdel-Salam E, Abdel-Meguid I, Korraa SS. Markers of degeneration and regeneration in Duchenne muscular dystrophy. Acta Myol. 2009;28(3):94–100.
9. Dumont NA, Wang YX, von Maltzahn J, Pasut A, Bentzinger CF, Brun CE, Rudnicki MA. Dystrophin expression in muscle stem cells regulates their polarity and asymmetric division. Nat Med. 2015;21(12):1455–63.
10. Ren S, Fu X, Guo W, Bai R, Li S, Zhang T, Liu J, Wang Z, Zhao H, Suo S, et al. Profound cellular defects attribute to muscular pathogenesis in the rhesus monkey model of Duchenne muscular dystrophy. Cell. 2024;187(23):6669–e66866616.
11. Esper ME, Brun CE, Lin AYT, Feige P, Catenacci MJ, Sincennes MC, Ritso M, Rudnicki MA. Intrinsic Muscle Stem Cell Dysfunction Contributes to Impaired Regeneration in the mdx Mouse. J Cachexia Sarcopenia Muscle. 2025;16(1):e13682.
12. Esper ME, Lin AYT, Bennett D, Rudnicki MA. Intrinsic dysfunction in muscle stem cells lacking dystrophin begins during secondary myogenesis. Nat Commun. 2025;16(1):10031.
13. Granet JA, Robertson R, Cusmano AA, Filippelli RL, Lorenz TO, Li S, Yaqubi M, Stratton JA, Chang NC. Muscle stem cells in Duchenne muscular dystrophy exhibit molecular impairments and altered cell fate trajectories impacting regenerative capacity. Cell Death Dis. 2025;16(1):437.
14. Ross J, Benn A, Jonuschies J, Boldrin L, Muntoni F, Hewitt JE, Brown SC, Morgan JE. Defects in glycosylation impair satellite stem cell function and niche composition in the muscles of the dystrophic Large(myd) mouse. Stem Cells. 2012;30(10):2330–41.
15. Morgan J, Butler-Browne G, Muntoni F, Patel K. skeletal muscle stem cells involvement in pathology study g: 240th ENMC workshop: The involvement of skeletal muscle stem cells in the pathology of muscular dystrophies 25–27 January 2019, Hoofddorp, The Netherlands. Neuromuscul Disord. 2019;29(9):704–15.
16. Boldrin L, Zammit PS, Morgan JE. Satellite cells from dystrophic muscle retain regenerative capacity. Stem Cell Res. 2015;14(1):20–9.
17. Tierney MT, Stec MJ, Rulands S, Simons BD, Sacco A. Muscle Stem Cells Exhibit Distinct Clonal Dynamics in Response to Tissue Repair and Homeostatic Aging. Cell Stem Cell. 2018;22(1):119–e127113.
18. Hughes SM, Escaleira RC, Wanders K, Koth J, Wilkinson DG, Xu Q. Clonal behaviour of myogenic precursor cells throughout the vertebrate lifespan. Biol Open. 2022;11(8):1–15.
19. Gurevich DB, Nguyen PD, Siegel AL, Ehrlich OV, Sonntag C, Phan JM, Berger S, Ratnayake D, Hersey L, Berger J, et al. Asymmetric division of clonal muscle stem cells coordinates muscle regeneration in vivo. Science. 2016;353(6295):aad9969.
20. Kuang S, Kuroda K, Le Grand F, Rudnicki MA. Asymmetric self-renewal and commitment of satellite stem cells in muscle. Cell. 2007;129(5):999–1010.

21. Feige P, Brun CE, Ritso M, Rudnicki MA. Orienting Muscle Stem Cells for Regeneration in Homeostasis, Aging, and Disease. Cell Stem Cell. 2018;23(5):653–64.
22. Molina T, Fabre P, Dumont NA. Fibro-adipogenic progenitors in skeletal muscle homeostasis, regeneration and diseases. Open Biol. 2021;11(12):210110.
23. Dumont NA, Rudnicki MA. Targeting muscle stem cell intrinsic defects to treat Duchenne muscular dystrophy. NPJ Regen Med. 2016;1:16006.
24. Dubuisson N, Versele R, Planchon C, Selvais CM, Noel L, Abou-Samra M. Davis-Lopez de Carrizosa MA: Histological Methods to Assess Skeletal Muscle Degeneration and Regeneration in Duchenne Muscular Dystrophy. Int J Mol Sci. 2022;23(24).
25. Schiaffino S, Gorza L, Sartore S, Saggin L, Carli M. Embryonic myosin heavy chain as a differentiation marker of developing human skeletal muscle and rhabdomyosarcoma. A monoclonal antibody study. Exp Cell Res. 1986;163(1):211–20.
26. Janghra N, Morgan JE, Sewry CA, Wilson FX, Davies KE, Muntoni F, Tinsley J. Correlation of Utrophin Levels with the Dystrophin Protein Complex and Muscle Fibre Regeneration in Duchenne and Becker Muscular Dystrophy Muscle Biopsies. PLoS ONE. 2016;11(3):e0150818.
27. Bencze M, Periou B, Baba-Amer Y, Authier FJ. Immunolabelling Myofiber Degeneration in Muscle Biopsies. J Vis Exp. 2019(154).
28. Andersen JT, Sandlie I. The versatile MHC class I-related FcRn protects IgG and albumin from degradation: implications for development of new diagnostics and therapeutics. Drug Metab Pharmacokinet. 2009;24(4):318–32.
29. Terrill JR, Bautista APR, Tsioutsias I, Grounds MD, Arthur PG. Oxidised Albumin Levels in Plasma and Skeletal Muscle as Biomarkers of Disease Progression and Treatment Efficacy in Dystrophic mdx Mice. Antioxid (Basel). 2024;13(6).
30. Markati T, Oskoui M, Farrar MA, Duong T, Goemans N, Servais L. Emerging therapies for Duchenne muscular dystrophy. Lancet Neurol. 2022;21(9):814–29.
31. Mayhew AG, Signorovitch J, Johnson M, Frean M, Ward SJ, Posner N, Merla V, Mahn M, Stimpson G, Guglieri M, et al. Visualizing ambulatory performance by age and rates of decline among patients with Duchenne muscular dystrophy. J Neuromuscul Dis. 2025;12(3):435–40.
32. Wang C, Yue F, Kuang S. Muscle Histology Characterization Using H&E Staining and Muscle Fiber Type Classification Using Immunofluorescence Staining. Bio Protoc. 2017;7(10).
33. Guiraud S, Davies KE. Regenerative biomarkers for Duchenne muscular dystrophy. Neural Regen Res. 2019;14(8):1317–20.
34. Bettica P, Petrini S, D'Oria V, D'Amico A, Catteruccia M, Pane M, Sivo S, Magri F, Brajkovic S, Messina S, et al. Histological effects of givinostat in boys with Duchenne muscular dystrophy. Neuromuscul Disord. 2016;26(10):643–9.
35. Briguet A, Courdier-Fruh I, Foster M, Meier T, Magyar JP. Histological parameters for the quantitative assessment of muscular dystrophy in the mdx-mouse. Neuromuscul Disord. 2004;14(10):675–82.
36. Dumont NA, Bentzinger CF, Sincennes MC, Rudnicki MA. Satellite Cells and Skeletal Muscle Regeneration. Compr Physiol. 2015;5(3):1027–59.
37. Kiriaev L, North KN, Head SI, Houweling PJ. Twisting Paths: The Paradox of Fiber Branching in Muscle Regeneration. Int J Mol Sci. 2026;27(2).
38. Cooper ST, Head SI. Membrane Injury and Repair in the Muscular Dystrophies. Neuroscientist. 2015;21(6):653–68.
39. Tulangekar A, Sztal TE. Inflammation in Duchenne Muscular Dystrophy-Exploring the Role of Neutrophils in Muscle Damage and Regeneration. Biomedicines. 2021;9(10).
40. Porter JD, Khanna S, Kaminski HJ, Rao JS, Merriam AP, Richmonds CR, Leahy P, Li J, Guo W, Andrade FH. A chronic inflammatory response dominates the skeletal muscle molecular signature in dystrophin-deficient mdx mice. Hum Mol Genet. 2002;11(3):263–72.
41. Ng SY, Ljubicic V. Recent insights into neuromuscular junction biology in Duchenne muscular dystrophy: Impacts, challenges, and opportunities. EBioMedicine. 2020;61:103032.
42. Krishnan VS, Aartsma-Rus A, Overzier M, Lutz C, Bogdanik L, Grounds MD. Implications of increased S100beta and Tau5 proteins in dystrophic nerves of two mdx mouse models for Duchenne muscular dystrophy. Mol Cell Neurosci. 2020;105:103484.
43. Schiaffino S, Gorza L, Pitton G, Saggin L, Ausoni S, Sartore S, Lomo T. Embryonic and neonatal myosin heavy chain in denervated and paralyzed rat skeletal muscle. Dev Biol. 1988;127(1):1–11.
44. Ringel SP, Bender AN, Engel WK. Extrajunctional acetylcholine receptors. Alterations in human and experimental neuromuscular diseases. Arch Neurol. 1976;33(11):751–8.
45. Guillon E, Bacar H, Gilquin L, Sasaki T, Mourikis P, Ruggiero F. Unraveling the matrisome signatures of quiescent and activated muscle stem cells. Stem Cell Rep. 2025;20(10):102635.
46. Long AM, Lee G, Demonbreun AR, McNally EM. Extracellular matrix contribution to disease progression and dysfunction in myopathy. Am J Physiol Cell Physiol. 2023;325(5):C1244–51.
47. Swandulla D, Ohlendieck K. Proteomic profiling of the extracellular matrix in skeletal muscle. Adv Clin Chem. 2025;129:53–122.
48. Mavropalias G, Boppart M, Usher KM, Grounds MD, Nosaka K, Blazevich AJ. Exercise builds the scaffold of life: muscle extracellular matrix biomarker responses to physical activity, inactivity, and aging. Biol Rev Camb Philos Soc. 2023;98(2):481–519.
49. Cai L, Shi L, Peng Z, Sun Y, Chen J. Ageing of skeletal muscle extracellular matrix and mitochondria: finding a potential link. Ann Med. 2023;55(2):2240707.
50. Dadgar S, Wang Z, Johnston H, Kesari A, Nagaraju K, Chen YW, Hill DA, Partridge TA, Giri M, Freishtat RJ, et al. Asynchronous remodeling is a driver of failed regeneration in Duchenne muscular dystrophy. J Cell Biol. 2014;207(1):139–58.
51. Duong L, Radley HG, Lee B, Dye DE, Pixley FJ, Grounds MD, Nelson DJ, Jackaman C. Macrophage function in the elderly and impact on injury repair and cancer. Immun Ageing. 2021;18(1):4.
52. Komaki H. Duchenne muscular dystrophy: Evolving therapeutic strategies and multidimensional evaluation approaches. Brain Dev. 2025;47(5):104397.
53. Deng J, Zhang J, Shi K, Liu Z. Drug development progress in duchenne muscular dystrophy. Front Pharmacol. 2022;13:950651.
54. McDonald CM, Guglieri M, Vucinic D, Acsadi G, Brandsema JF, Bruno C, Finanger EL, Harper A, Lobato ML, Masson R, et al. Long-Term Evaluation of Givinostat in Duchenne Muscular Dystrophy, and Natural History Comparisons. Ann Clin Transl Neurol. 2025;12(11):2335–48.

Publisher's Note